Nanoscale

Accepted Manuscript

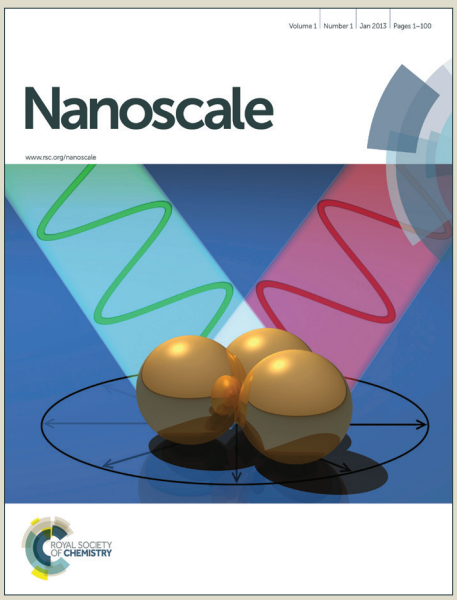

ROYAL SOCIETY OF CHEMISTRY

www.rsc.org/nanoscale

Journal Name

RSCPublishing

ARTICLE

Stepwise assembly of cross-linked free-standing nanoparticle sheet with controllable shape†

Cite this: DOI: 10.1039/xoxxoooooox

Hui Zhang,[‡a] Mei Liu,[‡a] Tian Zhou,[b] Bin Dong,*[a] and Christopher Y. Li*[b]

Received ooth
Accepted ooth

DOI: 10.1039/xoxxoooooox

www.rsc.org/

In this paper, we report a free-standing thin lamella consisting of nanoparticles with controllable shape. Self-assembly technique is utilized to obtain this sheet in a step by step fashion with nanoparticle and polymer single crystal as the basic building blocks. Inside the thin lamella, nanoparticles are not only immobilized on the surface of a polymer single crystal, which functions as a template, but also interconnected by a bifunctional crosslinker, *i.e.* 1,6-hexane dithiol. As a consequence, the nanoparticle lamella is crosslinked and can not be destructed by solvent and heat treatment. This fabrication strategy is generally applicable and can be applied to a variety of different nanoparticles with various properties, including catalytically active platinum nanoparticles, superparamagnetic iron oxide nanoparticles or luminescent quantum dots, and different types of polymer single crystals, such as hexagonal polycaprolactone and square-shaped polyethylene glycol ones. Based on the abundant properties originated from both nanoparticles and polymer single crystals, we have demonstrated that the resulting ensemble can function as recyclable catalytically active materials or magnetically responsive luminescent materials.

Introduction

In recent years, nanoparticles have attracted more and more attentions.[1,2] Because of the size effect, nanoparticles often exhibit fascinating optical, magnetic and electronic properties.[3-5] Nanoparticles bearing these unique properties have been exploited in potential applications ranging from imaging,[6] magnetic storage[7] to nanoparticle nanowire conductor for nanodevices.[8] Their extremely high surface area to volume ratio makes them particularly useful in catalysis and sensing applications.[9] In order to utilize the nanoparticles in real applications, it is desirable to assemble the nanoparticles in a controllable fashion.[10-12] To this end, researchers have focused on the organization of larger nanostructures comprising nanoparticles and their unique collective properties originated from individual nanoparticle.[13,14] Examples include wires consist of nanoparticles for nanoelectronics[15] or nanoparticle arrays for plasmonic devices, *etc.*[16] Up to now, scientists have developed a variety of different strategies for the controlled nanoparticle self-assembly.[17] For example, DNA based method can be utilized to control the organization of nanoparticle to form well defined structures.[18] Murray *et al.* have developed a slow evaporation method for the fabrication of nanoparticle based superlattices.[19] Wang *et al.* have utilized the interfacial self-assembly to construct nanoparticle membranes.[20] The challenge associated with these methods is either they are costly or the nanoparticle ensembles lack well defined shape.

Polymer single crystals are two-dimensional thin lamellae comprising long polymeric chains folded back and forth with a thickness of approximately 10 nm, which is normally obtained by solution crystallization method.[21] Depending on the crystallization conditions, the size of the polymer single crystal is controllable. The lateral dimension can be tuned between several tens of nanometers and hundreds of micrometers. When end functionalized polymeric material is utilized, due to the structure difference between the end functional groups and the polymer backbone, the end functional groups (such as thiol, hydroxyl, alkoxysilane, etc.) are excluded onto the surface of the polymer single crystals during the crystallization process.[22] By utilizing the interactions between these functional groups and the nanoparticles, a variety of different nanoparticles can be introduced onto the surface of polymer single crystal.[23] Based on this property, polymer single crystal can be utilized as a versatile two dimensional (2D) template to obtain various nanoparticle structures, including Janus nanoparticles,[24,25] nanoparticle dimers and chains[26,27] and hetero nanoparticles.[28] It has been demonstrated that polymer single crystals can potentially be utilized as recyclable catalyst support.[29] However, one drawback for these 2D hybrid ensembles is that the single crystal-forming polymer used are susceptible to solvent and heat treatment, making them less stable and more suitable as a sacrificial template instead of a stable support.

In this paper, we report the fabrication of mechanically robust, free-standing, regular shaped nanoparticle ensembles. A typical 2D ensemble consist of four different components, *i.e.* bi-functional polycaprolactone (PCL) single crystal or polyethylene glycol (PEG) single crystal, 1,6-hexane dithiol (HDT) and two different types of nanoparticles, *i.e.* magnetic iron oxide nanoparticle (Fe_3O_4NP) with metallic platinum nanoparticle (PtNP) or semiconducting cadmium selenide nanoparticle (CdSeNP). The 2D single crystal functions as a template for the nanoparticle assembly; the nanoparticles, together with HDT, synergistically crosslink the single crystal, leading to a class of robust, 2D hybrid materials. Two different nanoparticle ensembles have been successfully fabricated, *i.e.* Fe_3O_4NP and PtNP crosslinked with PCL single crystal and HDT (denoted as Fe_3O_4-

PCL-Pt) in the shape of a hexagon and Fe_3O_4NP and CdSeNP cross-linked with PEG single crystal and HDT (abbreviated as Fe_3O_4-PEG-CdSe) in the shape of a square. Because of the cross-linked structure, the resulting hybrid ensemble is stable at elevated temperature and insoluble in solvents. The structural stability, together with the collective properties from both nanoparticles and polymer single crystals, lead to a few value added properties such as improved recyclability as magnetically recyclable catalyst and magnetically responsive luminescence property.

Experimental

Materials

ε-Caprolactone, 2-mercaptoethanol, 1-butanol, pentyl acetate, *Candida antarctica* lipase B (CALB), 10 nm Fe_3O_4NP, 3 nm and 5 nm Lumidot CdSeNP, HDT and 4-nitrophenol were obtained from Sigma Aldrich Company. Alpha, omega-bis-mercapto polyethylene glycol (M_w=3k) was purchased from Iris biotech GMBH. *α*-Hydroxyl-*ω*-thiol terminated PCL and 3 nm PtNP were synthesized following literature methods.[30,31]

Fabrication Method for Fe_3O_4-PCL-Pt:

The fabrication of PCL single crystals was based on self-seeding technique.[32] In a typical experiment, PCL (9 mg) is first dissolved in 1-butanol (30 g) at 60 ˚C for 10 min, after which, the solution was cooled to 5 ˚C and isothermally crystallized at 5 ˚C for 2 h. The crystal seeds were obtained by re-heating the solution to 46 ˚C for 10 min. PCL single crystals were formed by allowing the above solution to crystallize at 22 ˚C for 24 h. Uncrystallized PCL was removed by isothermal filtration. To attach 10 nm Fe_3O_4NP, PCL single crystal was first dispersed in pentyl acetate by centrifugation method. Fe_3O_4NP solution was then mixed with PCL single crystal's pentyl acetate solution with 1 to 5 weight ratio and stirred for 24 h. Free Fe_3O_4NPs were removed by centrifugation. Fe_3O_4NP decorated PCL single crystal was then dispersed in pentyl acetate containing 1 mg/ml HDT and stirred for 24 h. Excess HDT was removed by centrifugation method. Fe_3O_4NP-decorated PCL single crystal with adsorbed HDT was then dispersed in methanol containing PtNP for 24 h. After removing the free PtNPs by centrifugation, the Fe_3O_4-PCL-Pt was obtained.

Fabrication Method for Fe_3O_4-PEG-CdSe

PEG single crystal was obtained by first dissolving 16 mg PEG in 30 g pentyl acetate at 60 ˚C for 10 min. After cooling the solution for 2 h at 5 ˚C, it was re-heated at 45 ˚C for 10 min to obtain the crystal seeds. PEG single crystal was then obtained at 22 ˚C for 24 h. Isothermal filtration was utilized to remove the uncrystallized PEG. PEG single crystal's pentyl acetate solution was then mixed with Fe_3O_4NP's toluene solution with 10 to 1 weight ratio for 24 h. Excess Fe_3O_4NPs were removed by centrifugation. HDT decoration on Fe_3O_4NP surface was achieved by treating Fe_3O_4NP decorated PEG single crystal with 1mg/ml HDT for 24 h. The excess amount of HDT was removed by centrifugation method. After re-dispersing the Fe_3O_4NP decorated PEG single crystal with adsorbed HDT in pentyl acetate, it was mixed with CdSeNP's toluene solution with 6 to 1 volume ratio and stirred for 24 h. Un-attached CdSeNP was removed through centrifugation, leading to the formation of Fe_3O_4-PEG-CdSe.

Test of catalytic behaviour of Fe_3O_4-PCL-Pt

30 µL of 2 mM 4-nitrophenol aqueous solution was added to 1.67 mL of deionized water. Fe_3O_4-PCL-Pt solution, originally dispersed in pentyl acetate, was re-dispersed in deionized water by centrifugation. 250 µL of Fe_3O_4-PCL-Pt was added to the dilute 4-nitrophenol solution. After the addition of 2 mL of 0.06 M $NaBH_4$ solution, the final solution was examined by UV-Vis Spectrometer. Deionized water used in this catalysis experiment was purged in nitrogen gas for at least 10 min to help remove oxygen.

Magnetic recovery test for Fe_3O_4-PCL-Pt catalyst

30 µL of 2 mM 4-nitrophenol solution was added to 1.67 mL of deionized water. Fe_3O_4-PCL-Pt was centrifuged at 3000 rpm for 5 min and the precipitate was re-dispersed in deionized water. 250 µL of ten times more concentrated Fe_3O_4-PCL-Pt was added to the diluted 4-nitrophenol solution. After adding 2 mL of 0.06 M $NaBH_4$ solution, the mixture was examined using a UV-Vis spectrometer. After the UV-Vis experiments, the sample was separated using a 1.5 Tesla rare earth metal magnet. The supernatant was removed and the precipitate was washed with de-ionized water, which was then re-filled with 1.67 mL deionized water, 30 µL of 2 mM 4-nitrophenol solution and 2 mL of fresh 0.06 M $NaBH_4$ solution. The catalytic process was monitored again by UV-Vis spectrometer. This procedure was repeated until the desired number of recovery cycles had been obtained. The recorded UV-Vis spectra were utilized to estimate the completion of the catalytic reaction after each cycle. Deionized water had been purged in nitrogen gas for at least 10 min to remove oxygen.

Characterizations

UV-Vis spectra were obtained on a Lambda 750 Spectrometer. TEM experiments were performed on a FEI Tecnai-F20 TEM operated at an acceleration voltage of 200 kV. TEM samples were prepared by drop-casting single crystal suspension on a carbon-coated nickel grid. Solvent was allowed to evaporate before TEM examination. Fluorescent images are captured using a Leica DM4000M fluorescence microscope. Atomic force microscopy (AFM) images are obtained on a Bruker Dimension Scanning Probe Microscopy. The magnetic manipulation of Fe_3O_4-PEG-CdSe was realized by applying a 1.5 Tesla rare earth metal magnet near the side wall of the test tube, which was then captured by using a CCD camera.

Results and discussion

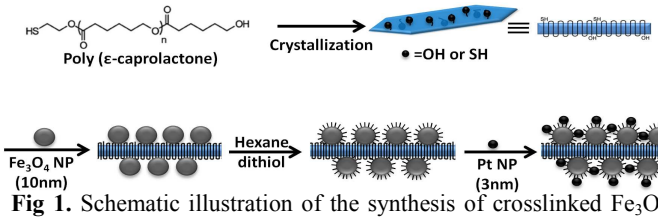

Fig 1. Schematic illustration of the synthesis of crosslinked Fe_3O_4-PCL-Pt nanosheet.

Fig. 1 illustrates the fabrication process. In a typical experiment, PCL was first crystallized to form polymer single crystals using solution crystallization method.[33] Due to the property difference between the polymer main chain and the chain end, the end functional group, *i.e.* –OH and –SH are exposed to the surface of the polymer single crystal during the solution crystallization process,[22] leading to the formation of the surface functionalized, hexagonal PCL single crystal with a thickness of approximately 8 nm.[29] Fig. 2a shows a typical low magnification TEM image of one PCL single crystal. We have examined the PCL single crystal using AFM. As shown in Fig. 2b, the thickness of PCL single crystal is approximately 8 nm. Since PCL (M_n=9.2kg/mol) possesses a two-chain orthorhombic unit cell with parameter of a=0.748 nm, b=0.498 nm and c=1.726 nm,[34] the areal density of surface –OH and –SH functional groups can be estimated to be approximately 0.3/nm^2 by assuming all functional groups are excluded onto the surface of PCL single crystal.[35] On the other hand, Fe_3O_4NPs have been reported to form chemical bonding with both –OH and –SH functional groups.[36] Therefore, such a high functional group density on the PCL single crystal surface implies that it can be utilized as a crosslinker for

Fe_3O_4NP. By treating PCL single crystal with excess amount of Fe_3O_4NP for saturated adsorption, the structure of two dense layers of Fe_3O_4NP sandwiching the PCL single crystal is formed,[32,37,38] as illustrated in Fig. 1. Fig. 2c indicates the TEM image of the dense packing Fe_3O_4NPs on PCL single crystal surface. By analysing the TEM image, the surface coverage density of Fe_3O_4NP can be estimated to be approximately 7500 μm^{-2}. AFM is utilized to study the thickness changes after Fe_3O_4NP adsorption. As illustrated in Fig. 2d, the thickness increases to around 28 nm, which is about the summation of the thickness of PCL crystal (8 nm) and 2 times the average diameter of Fe_3O_4NP, indicating the formation of the sandwich structure (Fig. 1). In order to confirm the PCL single crystal has crosslinked the nanoparticles on the top and bottom surfaces. We have performed a control experiment by dissolving away the PCL single crystal in chloroform. As can be seen from Fig. S1 in ESI†, the formation of Fe_3O_4NP dimer structures is observed, indicating that PCL single crystal can efficiently crosslink the top and bottom Fe_3O_4NPs. This result is in accordance with the literature in which the bi-surface functionalized polymer single crystal can be utilized to fabricate dumbbell nanoparticles.[27] This control experiment also shows that, in the present case, using Fe_3O_4NP is not sufficient to crosslink the entire ensemble. In order to fully crosslink the whole structure, after the Fe_3O_4NP immobilization, bifunctional crosslinker, *i.e.* HDT,[39] is introduced onto the surface of Fe_3O_4NP followed by the addition of a second nanoparticle, *e.g.* 3 nm PtNP. PtNPs are then immobilized onto the surface of Fe_3O_4NP though Pt-S bonding. Due to the high adsorption density of 10 nm Fe_3O_4NP (Fig. 2c), the PtNP can bridge the gap between Fe_3O_4NPs and crosslink them on the PCL single crystal surface, as indicated in Fig. 2e, resulting in the formation of crosslinked nanoparticle ensemble consisting of two different types of nanoparticles, *i.e.* Fe_3O_4NP and PtNP, with PCL single crystal and HDT as the inter- and intra- particle layer crosslinkers.[39]

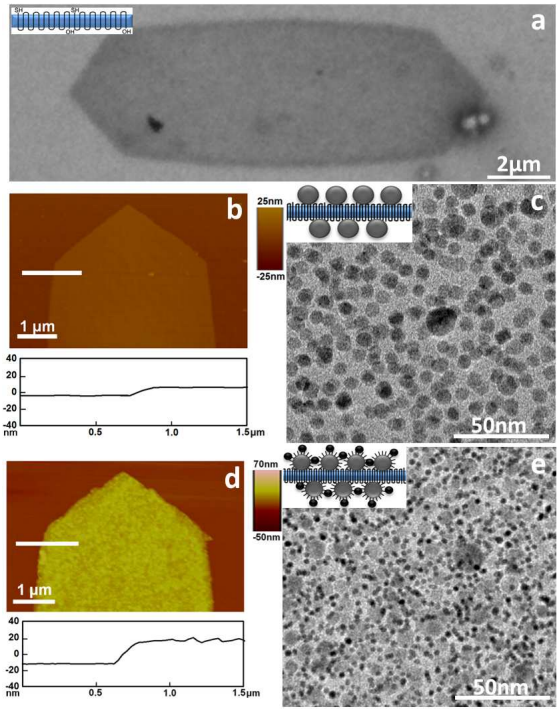

Fig. 2 (a) A typical TEM image indicating a hexagonal PCL single crystal. (b) AFM image and the corresponding section analysis of a PCL single crystal. (c) TEM image of the PCL single crystal with dense layers of Fe_3O_4NPs covering both the top and bottom surfaces. (d) AFM image and section analysis of Fe_3O_4NP decorated PCL single crystal. (e) TEM image of Fe_3O_4-PCL-Pt.

After the second crosslinking step with HDT and PtNP, the resulting Fe_3O_4-PCL-Pt is no longer soluble in chloroform, a good solvent for both the nanoparticles and the polymer. Fig. 3b indicates the Fe_3O_4-PCL-Pt after being immersed in chloroform. As compared to the original Fe_3O_4-PCL-Pt which is shown in Fig. 3a, the structure of Fe_3O_4-PCL-Pt remains intact after chloroform treatment. Furthermore, we have heated this crosslinked nanoparticle ensemble to 100 °C. As shown in Fig. 3c, the structure of Fe_3O_4-PCL-Pt is similar to that shown in Fig. 3a, indicating heat has negligible influence on the structure of Fe_3O_4-PCL-Pt. Note that PCL starts dissolving in solvent around 40 ˚C.[23] In order to confirm the structural integrity at microscale, we have also examined the samples after chloroform and heat treatment under TEM. As can be seen from Fig. 3d and 3e, the microstructure is the same as the one shown in Fig. 2e, indicating both the macroscopic and the microscopic structures are intact. Therefore, the above results confirm the crosslinked structure of Fe_3O_4-PCL-Pt.

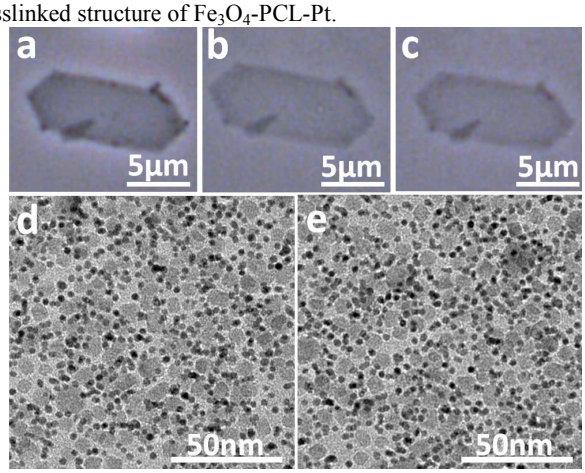

Fig. 3 Optical microscopic image showing a Fe_3O_4-PCL-Pt before (a) and after chloroform (b) and heat treatment (c). TEM images showing the Fe_3O_4-PCL-Pt after (d) chloroform and (e) heat treatment.

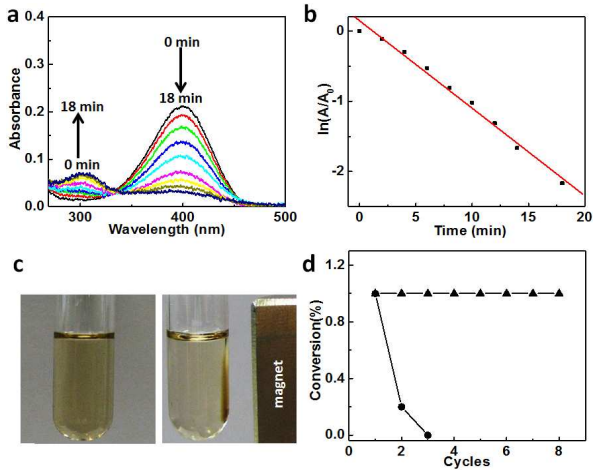

Fig. 4 (a) UV-Vis spectra of 4-nitrophenol reduction reaction for Fe_3O_4-PCL-Pt during 18 min reaction with 2 min interval and (b) linear relationship of $\ln(A/A_0)$ as a function of time. (c) Photo showing the Fe_3O_4-PCL-Pt dispersed in 4-nitrophenol aqueous solution (left), which can be quickly separated out in the presence of a magnet (right). (d) Conversion of 4-nitrophenol in eight successive recycling cycles at 50 ˚C in the presence of crosslinked Fe_3O_4-PCL-Pt (triangle) as opposed to that in the case of the uncrosslinked one (circle).

The crosslinked Fe_3O_4-PCL-Pt consists of both metallic nanoparticle (PtNP) and magnetically responsive material (Fe_3O_4NP), which makes it an ideal candidate for recyclable nanocatalyst. We have adopted the 4-nitrophenol reduction as the model reaction to assess the catalytic activity of Fe_3O_4-PCL-Pt.[40] 4-Nitrophenol is an important intermediate for the chemical synthesis of paracetamol.[41] The reduction of 4-nitrophenol to 4-aminophenol by sodium borohydride has no side reaction and can be easily traced using UV-Vis spectrometer. Fig. 4a shows the successive UV-Vis spectra taken at 2 min interval of 4-nitrophenol reduction reaction in the presence of Fe_3O_4-PCL-Pt. By placing Fe_3O_4-PCL-Pt into the 4-nitrophenol solution, the characteristic peak at 400 nm, which corresponds to 4-nitrophenol, decreases gradually. Simultaneously, the peak at 300 nm, which is the absorption of 4-aminophenol, increases accordingly. The reaction completes within 20 mins and the formation of an isosbestic point is clearly visible in Fig. 4a, indicating there is no side reaction. The absorption peak intensity in the UV-Vis spectra can be utilized to assess the reaction rate. As shown in Fig. 4b, the apparent rate constant can be estimated to be around 0.24 min^{-1}, indicating the high catalytic activity of Fe_3O_4-PCL-Pt. The normalized rate constant is estimated to be approximately 0.04 s^{-1} g^{-1} L, which is comparable to that reported in the literatures.[29] Furthermore, due to the presence of Fe_3O_4NP, the whole catalyst system is magnetically recoverable. As can be seen from Fig. 4c, Fe_3O_4-PCL-Pt can be quickly separated out from the reaction solution using a magnet, which allows us to test the recyclability of current catalyst system. We increased the amount of catalyst added into the 4-nitrophenol solution by 10 times so that the reaction can complete within 10 mins. After each cycle, the solution was sampled to confirm the completion of the reaction. Then the catalyst was quickly separated out under a magnetic field, rinsed with deionized water and re-dispersed in the reaction solution for the next cycle of catalysis. In addition, since Fe_3O_4-PCL-Pt is stable at elevated temperature due to the crosslinked structure, we evaluate its recyclability at 50 ˚C. As can be seen from Fig. 4d (the triangle curve), the catalyst can be successfully recycled for up to 8 times. During these 8 cycles, the reactions completed within 10 mins. After 8 cycles, the conversion was lower than 100% (around 80%), possibly because of the catalyst loss during the recycling process. We have examined the structure of Fe_3O_4-PCL-Pt after 8 cycles. As shown in Fig. S2 in ESI†, the change in the structure is negligible. Moreover, we have performed a control experiment by examining the catalyst recyclability based on a non-crosslinked structure similar to Fe_3O_4-PCL-Pt, *i.e.* both Fe_3O_4NPs and PtNPs were directly adsorbed onto PCL single crystal according to the literature method[29] without the addition of the crosslinker HDT. When tested under similar conditions (at 50 ˚C), Fe_3O_4-PCL-Pt can only be successfully recycled once, as shown in Fig. 4d (the circle curve). The conversion starts to fall after the first cycle, which can be attributed to the melting of the PCL single crystal, leading to the disassembly of the non-crosslinked structure. As a consequence, the whole system is no longer recyclable under magnetic field. This result is in sharp contrast to the 8 successful recycling of Fe_3O_4-PCL-Pt, demonstrating the superiority of the crosslinked system.

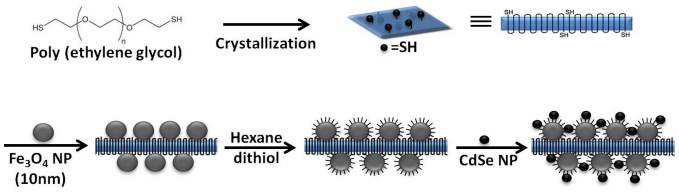

Fig. 5 Schematic illustration of the fabrication of Fe_3O_4-PEG-CdSe.

Because there are plenty of different types of polymer single crystals and nanoparticles, we further extended the current fabrication strategy to other hybrid systems. As a proof-of-concept, we have employed square-shaped PEG single crystals to fabricate the nanoparticle sheet following a similar protocol, as shown in Fig. 5. PEG single crystal with thiol surface functional groups was first obtained by self-seeding technique.[42] Fig. 6a illustrates a typical low magnification TEM image showing a single PEG single crystal exhibiting the square shape. The thickness of the PEG single crystal has been determined by AFM analysis to be around 8 nm (Fig. 6b). Fe_3O_4NP was then adsorbed onto the surface of the PEG single crystal, as illustrated in Fig. 6c. The surface coverage of Fe_3O_4NP on PEG single crystal (Fig. 6c) can be estimated to be around 7000 μm^{-2}, which is similar to that on PCL single crystal (Fig. 2c, 7500 μm^{-2}). The thickness of the Fe_3O_4NP decorated PEG crystal increases to around 28 nm (Fig. 6d), which is about the sum of the thickness of PEG crystal and 2 times the average diameter of Fe_3O_4NP, confirming the structure of two layers of 10 nm Fe_3O_4NP sandwiching the middle PEG single crystal. After the HDT adsorption which acts as a second crosslinker, 3 nm CdSeNP is adsorbed onto HDT to bridge the gap between Fe_3O_4NPs. Fig. 6e shows the TEM image of the Fe_3O_4-PEG-CdSe containing 3 nm CdSeNP (denoted as Fe_3O_4-PEG-$CdSe_3$). The surface is coated with a dense layer of nanoparticles. By utilizing high resolution TEM, the lattice structure from both Fe_3O_4NP and CdSeNP can be distinguished, *i.e.* 0.48 nm for Fe_3O_4NP (111) and 0.34 for CdSeNP (111), as shown in Fig. 6f.

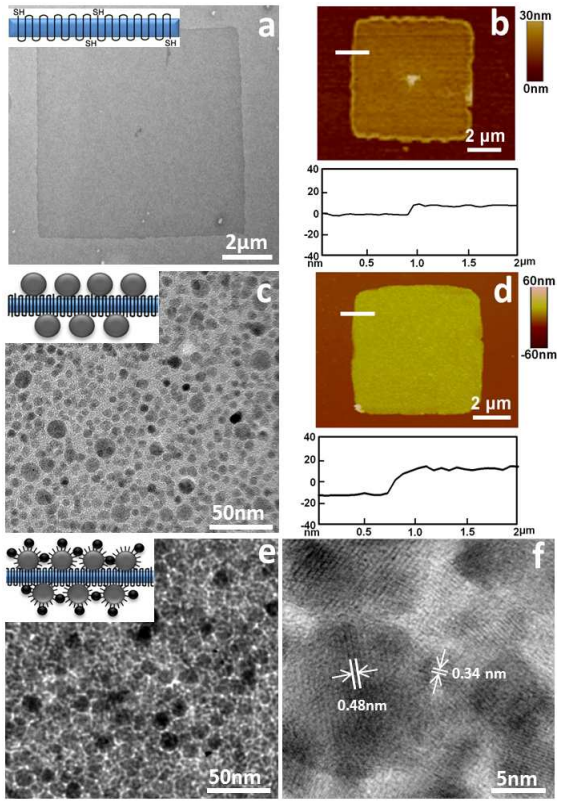

Fig. 6 (a) TEM, (b) AFM and the corresponding section analysis of a PEG single crystal, (c) TEM, (d) AFM and the corresponding section analysis of Fe_3O_4NP decorated PEG single crystal. (e) TEM image of Fe_3O_4-PEG-$CdSe_3$. (f) High resolution TEM image showing the lattice structure of Fe_3O_4 (111) and CdSe (111).

The resulting crosslinked structure, *i.e.* Fe_3O_4-PEG-$CdSe_3$, exhibits properties inherited from individual component. In order to examine their stability and study their property, we first dispersed

the Fe_3O_4-PEG-$CdSe_3$ in chloroform, a good solvent for both PEG single crystal, Fe_3O_4NP and CdSeNP.[43] Fe_3O_4-PEG-$CdSe_3$ was then dropcast on a silicon substrate for microscopic observation. As demonstrated in Fig. 7a, Fe_3O_4-PEG-$CdSe_3$ exhibits green fluorescence under UV light irradiation, which is the characteristic emission from 3 nm CdSeNP. The fluorescent magnetic nanoparticle composites have previously been fabricated by microemulsion[44] or sol-gel method,[45] which suffer from the fluorescence quenching due to the direct contact between Fe_3O_4NP and CdSeNP and the limited loading of CdSeNP. In current case, because of the presence of the spacer molecules in-between the nanoparticles and the high CdSeNP loading, the resulting Fe_3O_4-PEG-$CdSe_3$ is still fluorescent. In addition, it is notable that Fe_3O_4-PEG-$CdSe_3$ is in the shape of a square, which is originated from the shape of the PEG single crystal, indicating that chloroform has no adverse effect on the shape because of the crosslinked structure of Fe_3O_4-PEG-$CdSe_3$. By replacing 3 nm CdSeNP with a different sized CdSeNP (5 nm) as the final adsorbed nanoparticle, the emission color from the resulting Fe_3O_4-PEG-CdSe containing 5 nm CdSeNP (abbreviated as Fe_3O_4-PEG-$CdSe_5$) can be successfully tuned to red, as indicated in Fig. 7b. Furthermore, due to the presence of Fe_3O_4NP in the ensemble, Fe_3O_4-PEG-CdSe is magnetically responsive. Fig. 7c-d shows the CCD images of green colored Fe_3O_4-PEG-$CdSe_3$ and red colored Fe_3O_4-PEG-$CdSe_5$ in chloroform solution under the influence of an external magnetic field. The left and right images in Fig. 7c-d are captured in a direction parallel and perpendicular to the applied magnetic field, respectively. Moreover, since the fluorescent magnetic nanoparticle ensemble have been widely utilized in the literatures for the separation and detection of biomolecules,[46,47] the application of current Fe_3O_4-PEG-CdSe in such field is also greatly anticipated.

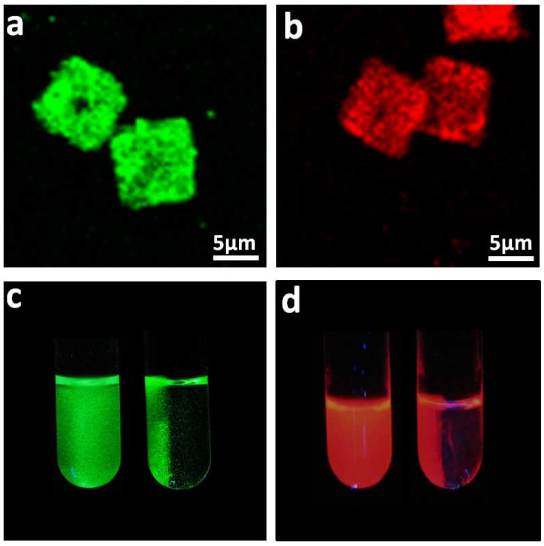

Fig. 7 Fluorescence microscopic images showing the square-shaped (a) Fe_3O_4-PEG-$CdSe_3$ and (b) Fe_3O_4-PEG-$CdSe_5$. CCD images shows the solution containing (c) Fe_3O_4-PEG-$CdSe_3$ and (d) Fe_3O_4-PEG-$CdSe_5$ when exposed to the magnetic field. Images are taken from the direction parallel (the left images in c and d) and perpendicular (the right images in c and d) to the applied magnetic field.

Conclusions

In conclusion, we report the novel synthesis of free standing nanoparticle thin lamella, which is realized through the utilization of a template based on polymer single crystals. Nanoparticles are not only immobilized onto the surface functionalized polymer single crystals through covalent bonding but also inter-connected through the utilization of a bifunctional linker, resulting in a robust crosslinked structure. As a consequence, the as-fabricated nanoparticle ensemble is stable in solvent and remains intact at elevated temperature. Due to the versatility in functionalities and structures from both nanoparticle and polymer single crystal building blocks, current crosslinked nanoparticle ensembles can not only be made into various shapes such as hexagon and square but also exhibit a variety of different functions including catalysis, magnetism and fluorescence, which make them potentially attractive for applications such as recyclable nanocatalyst and magnetically responsive luminescent material for separation and detection purpose.

Acknowledgements

This work is supported by the National Natural Science Foundation of China (Grant No. 21304064), the Natural Science Foundation of Jiangsu Province (Grant No. BK20130292), a Project Funded by the Priority Academic Program Development of Jiangsu Higher Education Institutions (PAPD), the Fund for Excellent Creative Research Teams of Jiangsu Higher Education Institutions, Jiangsu Key Laboratory for Carbon-Based Functional Materials & Devices and the project-sponsored by SRF for ROCS, SEM. CYL is grateful for the support from the National Science Foundation through grants CBET-1438240 and DMR-1308958.

Notes and references

[a]Institute of Functional Nano & Soft Materials (FUNSOM) and Collaborative Innovation Center (CIC) of Suzhou Nano Science and Technology, Soochow University, Suzhou, Jiangsu 215123, P. R. China, E-mail: bdong@suda.edu.cn
[b]Department of Materials Science and Engineering, Drexel University, Philadelphia 19104, USA, E-mail: chrisli@drexel.edu
[†]Electronic Supplementary Information (ESI) available: Fig. S1-S2. See DOI: 10.1039/b000000x/
[‡]These authors contributed equally to this work.

1. C. B. Murray, C. R. Kagan and M. G. Bawendi, *Annu. Rev. Mater. Sci.*, 2000, **30**, 545-610.
2. C. J. Murphy, A. M. Gole, J. W. Stone, P. N. Sisco, A. M. Alkilany, E. C. Goldsmith and S. C. Baxter, *Acc. Chem. Res.*, 2008, **41**, 1721-1730.
3. A. P. Alivisatos, *ACS Nano*, 2008, **2**, 1514-1516.
4. A. H. Lu, E. L. Salabas and F. Schuth, *Angew. Chem., Int. Ed.*, 2007, **46**, 1222-1244.
5. N. J. Halas, S. Lal, W. S. Chang, S. Link and P. Nordlander, *Chem. Rev.*, 2011, **111**, 3913-3961.
6. A. M. Smith and S. M. Nie, *Acc. Chem. Soc.*, 2010, **43**, 190-200.
7. H. Zeng, S. H. Sun, T. S. Vedantam, J. P. Liu, Z. R. Dai and Z. L. Wang, *Appl. Phys. Lett.*, 2002, **80**, 2583-2585.
8. J. X. Huang, R. Fan, S. Connor, P. D. Yang, *Angew. Chem., Int. Ed.*, 2007, **46**, 2414-2417.
9. A. Z. Moshfegh, *J. Phys. D: Appl. Phys.*, 2009, **42**, 233001.
10. A. R. Tao, J. X. Huang and P. D. Yang, *Acc. Chem. Res.*, 2008, **41**, 1662-1673.
11. W. L. Cheng, M. J. Campolongo, J. J. Cha, S. J. Tan, C. C. Umbach, D. A. Muller and D. Luo, *Nat. Mater.*, 2009, **8**, 519-525.
12. K. C. Ng, I. B. Udagedara, I. D. Rukhlenko, Y. Chen, Y. Tang, M. Premaratne and W. L. Cheng, *ACS Nano*, 2012, **6**, 925-934.
13. L. B. Wang, L. G. Xu, H. Kuang, C. L. Xu and N. A. Kotov, *Acc. Chem. Soc.*, 2012, **45**, 1916-1926.
14. K. J. Si, D. Sikdar, Y. Chen, F. Eftekhari, Z. Q. Xu, Y. Tang, W. Xiong, P. Z. Guo, S. Zhang, Y. R. Lu, Q. L. Bao, W. R. Zhu, M. Premaratne and W. L. Cheng, *ACS Nano*, 2014, **8**, 11086-11093.
15. T. Sato, H. Ahmed, D. Brown and B. F. G. Johnson, *J. Appl. Phys.*, 1997, **82**, 696-701.
16. L. Gunnarsson, E. J. Bjerneld, H. Xu, S. Petronis, B. Kasemo and M. Kall, *Appl. Phys. Lett.*, 2001, **78**, 802-804.

17. M. Grzelczak, J. Vermant, E. M. Furst and L. M. Liz-Marzan, *ACS Nano*, 2010, **4**, 3591-3605.
18. S. J. Tan, M. J. Campolongo, D. Luo and W. L. Cheng, *Nat. Nanotech.*, 2011, **6**, 268-276.
19. A. G. Dong, J. Chen, P. M. Vora, J. M. Kikkawa and C. B. Murray, *Nature*, 2010, **466**, 474-477.
20. H. W. Duan, D. Y. Wang, D. G. Kurth and H. Mohwald, *Angew. Chem., Int. Ed.*, 2004, **43**, 5639-5642.
21. P. Geil, *Polymer Single Crystals*, Robert Krieger Pub., Huntington, N. Y., 1973.
22. C. Y. Li, *J. Polym. Sci. Part B Polym. Phys.*, 2009, **47**, 2436-2440.
23. B. B. Wang, B. Li, R. C. M. Ferrier and C. Y. Li, *Macromol. Rapid Commun.*, 2010, **31**, 169-175.
24. B. Li and C. Y. Li, *J. Am. Chem. Soc.*, 2007, **129**, 12-13.
25. B. B. Wang, B. Li, B. Zhao and C. Y. Li, *J. Am. Chem. Soc.*, 2008, **130**, 11594-11595.
26. B. Dong, B. Li and C. Y. Li, *J. Mater. Chem.*, 2011, **21**, 13155-13158.
27. T. Zhou, B. Dong, H. Qi, H. K. Lau and C. Y. Li, *Nanoscale*, 2014, **6**, 4551-4554.
28. H. Zhang, B. Dong, T. Zhou and C. Y. Li, *Nanoscale*, 2012, **4**, 7641-7645.
29. B. Dong, D. L. Miller and C. Y. Li, *J. Phys. Chem. Lett.*, 2012, **3**, 1346-1350.
30. C. Hedfors, E. Ostmark, E. Malmstrom, K. Hult and M. Martinelle, *Macromolecules*, 2004, **38**, 647-649.
31. N. Toshima, M. Kuriyama, Y. Yamada and H. Hirai, *Chem Lett.*, 1981, 793-796.
32. B. Dong, W. D. Wang, D. L. Miller and C. Y. Li, *J. Mater. Chem*, 2012, **22**, 15526-15529.
33. D. J. Blundell and A. A. Keller, *Polym. Lett.*, 1966, **4**, 481-486.
34. H. L. Hu and D. L. Dorset, *Macromolecules*, 1990, **23**, 4604-4607.
35. T. Zhou, B. B. Wang, B. Dong and C. Y. Li, *Macromolecules*, 2012, **45**, 8780-8789.
36. J. C. Love, A. L. Estroff, J. K. Kriebel, R. G. Nuzzo and G. M. Whitesides, *Chem. Rev.*, 2005, **105**, 1103-1169.
37. B. Dong, T. Zhou, H. Zhang and C. Y. Li, *ACS Nano*, 2013, 7, 5192-5198.
38. M. Liu, L. M. Liu, W. L. Gao, M. D. Su, Y. Ge, L. L. Shi, H. Zhang, B. Dong and C. Y. Li, *Nanoscale*, 2014, **6**, 8601-8605.
39. H. Schlicke, J. H. Schroder, M. Trebbin, A. Petrov, M. Ijeh, H. Weller and T. Vossmeyer, *Nanotechnology*, 2011, **22**, 305303.
40. L. L. Shi, M. Liu, L. M. Liu, W. L. Gao, M. D. Su, Y. Ge, H. Zhang and B. Dong, *Langmuir*, 2014, **30**, 13456-13461.
41. S. Fazzini, M. C. Cassani, B. Ballarin, E. Boanini, J. S. Girardon, A. S. Mamede, A. Mignani and D. Nanni, *J. Phys. Chem. C*, 2014, **118**, 24538-24547.
42. B. Li, B. B. Wang, R. C. M. Ferrier and C. Y. Li, *Macromolecules*, 2009, **42**, 9394-9399.
43. B. B. Wang, B. Li, B. Dong, B. Zhao and C. Y. Li, *Macromolecules*, 2010, **43**, 9234-9238.
44. D. K. Yi, S. T. Selvan, S. S. Lee, G. C. Papaefthymiou, D. Kundaliya and J. Y. Ying, *J. Am. Chem. Soc.*, 2005, **127**, 4990-4991.
45. G. Ruan, G. Vieira, T. Henighan, A. R. Chen, D. Thakur, R. Sooryakumar and J. O. Winter, *Nano Lett.*, 2010, **10**, 2220-2224.
46. J. Hu, M. Xie, C. Y. Wen, Z. L. Zhang, H. Y. Xie, A. A. Liu, Y. Y. Chen, S. M. Zhou and D. W. Pang, *Biomaterials*, 2011, **32**, 1177-1184.
47. E. Q. Song, W. Y. Han, H. Y. Xu, Y. F. Jiang, D. Cheng, Y. Song and M. T. Swihart, *Chem. Eur. J.*, 2014, **20**, 14642-14649.